Numerical modeling of borehole-surface electromagnetic responses with 3-D finite difference method and comparison with physical simulations

HUI CAO[1], LIFENG MAO*[1], XUBEN WANG[1], ZHANXIANG HE[2] AND KUNPENG WANG[3]

1 Key Laboratory of Earth Exploration and Information Technology of MOE, Chengdu University of Technology, Chengdu, Sichuan 610059, China (caohui_cdut@163.com, mlf73@163.com)

2 BGP INC., China National Petroleum Corporation, Zhuozhou, Hebei 072750, China

3 School of Geophysics and Information Technology, China University of Geoscience, Beijing 100083, China

* Corresponding author

Received: April 15, 2013; Revised: September 27, 2013; Accepted: April July 14, 2014

ABSTRACT

Borehole-surface electromagnetic method (BSEM) is a high-accuracy electromagnetic prospecting method that uses AC-powered vertical finite line source as the excitation source. The observed surface electromagnetic field is inverted for the subsurface conductivity structure. In this paper, the total field is separated into a primary part, due to a horizontally layered host medium, and a secondary part due to 3-D heterogeneities. After solving for the primary field with an analytical method, the frequency-domain second-order differential equation for the secondary field is discretized by finite differences. A sparse matrix storage scheme is employed and a BiCGSSTAB(m) method with a diagonal matrix preconditioner is used to obtain the secondary field as well as the 3-D BSEM response of the model. We compare the result of anomalous responses of three-layered medium derived by 3-D forward modeling with the result of semi-analytical solution. We also perform physical simulation and 3-D numerical forward modeling based on similarity criterion. As a result, the shape of both anomalous response curves are the same, which validates the 3-D numerical simulation method. The anomalous fields of 3-D numerical forward and physical simulation share similar anomalous feature of symmetric bimodal structure that is consistent with its harmonic response curve. It demonstrates that borehole-surface electromagnetic method can be used not only for prospection by employing a multi-frequency response, but also can provide multi-angle information about subsurface anomaly by varying relative depths of vertical finite line source in the borehole.

Keywords: borehole-surface electromagnetic method; finite difference method; numerical simulation; physical simulation

1. INTRODUCTION

Borehole-surface electromagnetic method (BESM) is a geophysical prospecting method to evaluate conditions of reservoir by inverting response components of the electromagnetic field measured on the surface for the subsurface electrical structure. The electromagnetic field is produced by signals with different frequencies sent from the vertical finite line source in the borehole at different depths. The 3-D forward simulation of this method plays a crucial role in understanding the features of borehole-surface electromagnetic response, guiding the construction method design, and also facilitating the interpretation of inversion.

Many authors already published a lot of studies in the field of 3-D electromagnetic forward modeling, such as the response simulation of 3-D target model with integral equation method (*Hohmann, 1975*; *Tripp et al., 1984*; *Newman et al., 1986*; *Xiong, 1992*), the simulation of complex geological geometry with finite element method featured with more flexible grid generation (*Badea et al., 2001*; *Mitsuhata and Uchida, 2004*; *Liu et al., 2008*), and the high-accuracy 3-D staggered-grid finite-difference method simulation in frequency-domain CSEM (*Streich, 2009*) with discretized second-order difference method.

Yet most studies on BSEM focus on borehole-surface DC resistivity methods. For instance, the study on DC-powered vertical finite line source with 3-D finite-difference and finite-element simulation method (*Xu et al., 2005*; *An et al., 2007*; *Ke et al., 2009*), the borehole-surface DC 3-D forward simulation with finite-difference method (*Wang et al., 2006*). However, due to heavy loads of calculation and the resulting accuracy problem, BSEM numerical simulation is less studied. For example, *Champagne (2001)* conducted a 3-D finite-difference numerical simulation with frequency higher than 2 MHz but they ignored the conduction currents of borehole-surface electromagnetic governing equations, and *Wang et al. (2007a,b)* adopted integral equation method of *Zhdanov and Fang (1997)* to perform a 3-D BSEM simulation but they neglected the displacement currents and their study also has the problem of increasing calculation complexity as the model grows.

In addition, there are also BSEM physical simulations, but due to limitations in experiment sites and equipments current experiments are all about simulations of BSEM DC resistivity (*Zhang et al., 1995*; *Wang et al., 2005*). Therefore, to explore BSEM response mechanism in depth and facilitate the prospecting of high-resistance anomalies, this paper performs a 3-D BSEM low-frequency simulation with vertical finite line source using staggered-grid finite-difference method to analyze the response curves in the profile of surface electromagnetic field, and then carries out flume experiments for BSEM response on the basis of similarity criterion of electromagnetic physical simulation.

2. BSEM FIELD GOVERNING EQUATIONS

We assume the surface as the *x*-*y* plane of a 3-D Cartesian coordinate system. The location of the borehole is the *z* axis, pointing down vertically .The conductivity of surrounding rock is σ and the conductivity of anomalous body is σ_1. Low-frequency AC is placed at the depth of h_1 and h_2 with current intensity of $I_0 e^{i\omega t}$ and polar length of

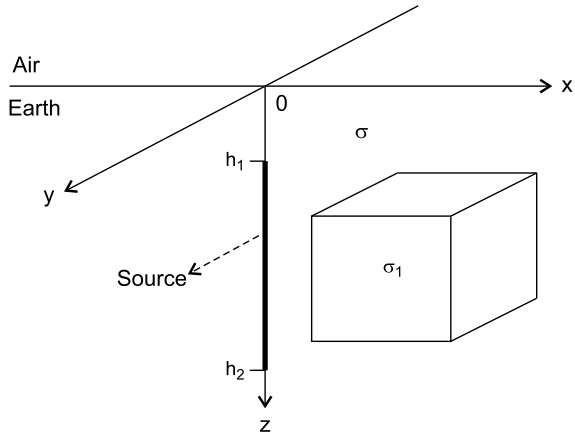

Fig. 1. Schematic presentation of detecting subsurface anomalies with BSEM. h_1, h_2: depths, σ_1: conductivity of anomalous body, σ: conductivity of surrounding rock.

$L = h_2 - h_1$. If $L > 0$, vertical finite line source is used as the excitation source. The electric field response components related to anomaly are received on surface at $Z = 0$. Fig. 1 demonstrates the setup of BSEM to detect subsurface anomalies.

Assume the magnetic permeability in the whole space is a constant which is near to the vacuum permeability of $\mu_0 = 4\pi \times 10^{-7}$ H/m. The scalar electrical conductivity is $\sigma(\boldsymbol{r})$ while and the angular frequency is ω. If the displacement currents can be ignored, integrating the Maxwell-Ampère circuital law with Maxwell-Faraday equation yields a second-order partial differential equation on electrical field and vertical primary electric current distribution:

$$\nabla \times \nabla \times \boldsymbol{E} + \mathrm{i}\omega\mu_0\sigma(\boldsymbol{r})\boldsymbol{E} = -\mathrm{i}\omega\mu_0\boldsymbol{J}_p\,, \tag{1}$$

where $\boldsymbol{J}_p$ represents the vertical finite line source and it is given by:

$$\boldsymbol{J}_p = I(\omega)\boldsymbol{I}\delta(z - z_s)\,, \tag{2}$$

where δ represents the Dirac's delta function, the location of source is $z_s = (0, 0, z_s)$, and $h_1 \le z_s \le h_2$.

Primary field conductivity σ_p and primary electric field $\boldsymbol{E}_p$ can satisfy Eq. (1), therefore we will use superposition principle to subtract primary field from the total field to get the secondary field $\boldsymbol{E}_s = \boldsymbol{E} - \boldsymbol{E}_p$. So Eq. (1) can be recast to give an equation of secondary field:

$$\nabla \times \nabla \times \boldsymbol{E}_s + \mathrm{i}\omega\mu_0\sigma(\boldsymbol{r})\boldsymbol{E}_s = -\mathrm{i}\omega\mu_0\left[\sigma(\boldsymbol{r}) - \sigma_p\right]\boldsymbol{E}_p\,. \tag{3}$$

In this case, the total field solution (Eq. 1) is transformed into the sum of $\boldsymbol{E}_s$ and $\boldsymbol{E}_p$. $\boldsymbol{E}_s$ can be obtained by numerical method while $\boldsymbol{E}_p$ by analytical method. This paper will, on the basis of 1-D analytical method that is provided by *Key (2009)*, calculate the

intensity of the primary electromagnetic field $\boldsymbol{f}$ of subsurface vertical electric dipole source in isotropic layered medium. We use *Guptasarma (1997)* method to calculate Hankel integral. Intensity of the primary electromagnetic field $\boldsymbol{F}$ excited by vertical finite line source will be computed using the line integral method in z direction (*Key, 2009*; *Cao et al., 2012*):

$$F = \int_{h_1}^{h_2} f(z)\,\mathrm{d}z\,. \tag{4}$$

3. FREQUENCY-DOMAIN FINITE-DIFFERENCE METHOD

Secondary field in this paper is obtained by frequency-domain finite-difference method. First, $\boldsymbol{E}_s$ in Eq. (3) will be expressed in 3 components to find the solution in 3 directions. For the convenience of writing, $\boldsymbol{E}_s$ will be referred to as $\boldsymbol{E}$ hereafter. In order to get finite-difference equations, non-uniform staggered-grid discretization (*Yee, 1966*) will be applied to Eq. (3). As shown in Fig. 2, for discretized cell at position (i, j, k), components of electric field will be sampled at the middle of edges of each cell while components of magnetic field will be at the center of faces of each cell.

Apply differential discretization to scalar values in Eq. (3) in x, y, z directions. Differential equation in x direction is:

$$\begin{aligned}
&\left\{\frac{\left(E^y_{i+1,j+1/2,k}-E^y_{i,j+1/2,k}\right)}{\Delta x_i}-\frac{\left(E^x_{i+1/2,j+1,k}-E^x_{i+1/2,j,k}\right)}{\Delta y_j}\right.\\
&\left.-\frac{\left(E^y_{i+1,j-1/2,k}-E^y_{i,j-1/2,k}\right)}{\Delta x_i}+\frac{\left(E^x_{i+1/2,j,k}-E^x_{i+1/2,j-1,k}\right)}{\Delta y_{j-1}}\right\}\frac{1}{\Delta' y_j}\\
&+\left\{\frac{\left(E^z_{i+1,j,k+1/2}-E^z_{i,j,k+1/2}\right)}{\Delta x_i}-\frac{\left(E^x_{i+1/2,j1,k+1}-E^x_{i+1/2,j,k}\right)}{\Delta z_k}\right.\\
&\left.-\frac{\left(E^z_{i+1,j,k-1/2}-E^z_{i,j,k-1/2}\right)}{\Delta x_i}+\frac{\left(E^x_{i+1/2,j1,k}-E^x_{i+1/2,j,k-1}\right)}{\Delta z_{k-1}}\right\}\frac{1}{\Delta' z_k}\\
&+\mathrm{i}\omega\mu_0\sigma_{i+1/2,j,k}E^x_{i+1/2,j,k}=-\mathrm{i}\omega\mu_0\left(\sigma_{i+1/2,j,k}-\sigma_{p(i+1/2,j,k)}\right)E^x_{p(i+1/2,j,k)}\,,
\end{aligned} \tag{5}$$

where Δx_i, Δy_j, Δz_k indicate the length of cell (i, j, k) in x, y, z directions, respectively. $\Delta' x_i$ is the distance between point $(i-(1/2), j, k)$ and point $(i+(1/2), j, k)$. $\Delta' y_j$ is the distance between point $(i, j-(1/2), k)$ and point

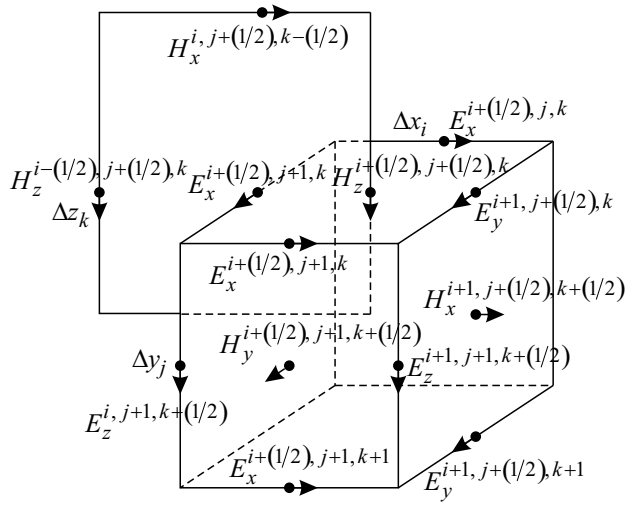

Fig. 2. Scheme of *Yee's (1966)* grid.

$\left(i,\, j+(1/2),\, k\right)$, while $\Delta' z_k$ is the distance between point $\left(i,\, j,\, k-(1/2)\right)$ and point $\left(i,\, j,\, k+(1/2)\right)$. The weighted conductivity is given by

$$\sigma_{i+(1/2),\,j,\,k} = \frac{\sigma_{i,\,j,\,k}\Delta y_j\,\Delta z_k + \sigma_{i,\,j-1,\,k}\Delta y_{j-1}\,\Delta z_k + \sigma_{i,\,j,\,k-1}\Delta y_j\,\Delta z_{k-1} + \sigma_{i,\,j-1,\,k-1}\Delta y_{j-1}\Delta z_{k-1}}{\left(\Delta y_j + \Delta y_{j-1}\right)\left(\Delta z_k + \Delta z_{k-1}\right)}.$$

When the subscript is changed accordingly, differential equations in y and z directions can be obtained. According to *Newman and Alumbaugh (1995)*, we employ staggered grid discretization to the model area including the air. The secondary field's boundary condition requires that tangential components of electric field vanishes. At last, the discretization of Eq. (2) produces a linear equation:

$$\mathbf{A}\boldsymbol{x} = \boldsymbol{b}, \tag{6}$$

where **A** is a complex symmetric matrix, $\boldsymbol{x}$ is the to-be-solved vector of electric field components in three directions of secondary field, while $\boldsymbol{b}$ contains the primary electric current distribution of the right side of Eq. (2) and also the boundary condition.

Suppose the computational space is partitioned into $Nx \times Ny \times Nz$ grid cells, Eq. (6) is a large-scale sparse symmetric system of linear equations. The order of its coefficient matrix **A** is $3Nx \times Ny \times Nz$. The non-zero elements of each row are less than 13**,** but the condition number is very large. So the linear equations are very ill-conditioned. In this paper, the resulting matrix Eq. (6) is solved by using the BICGSTAB(m) algorithm (*Freund R., 1993*; *Sleijpen and Fokkema, 1993*) with simple diagonal preconditioning. This solution is much stable than BICG or CGS method that needs no transpose and boasts higher calculation efficiency.

4. SOLUTION VERIFICATION

First of all, we will validate the 3-D finite-difference program by comparing it with the analytical solution of dipole 1-D program of *Key (2009)*, with vertical electric dipole being regarded as the excitation source. Given that the model has three layers, the upper layer is 300 m thick with a conductivity of 0.01 S/m; the middle layer is 400 m thick with a conductivity of 0.05 S/m; and the bottom layer conductivity is 0.01 S/m. The conductivity of the air is 10^{-12} S/m, and the vertical finite line source is 1 m long from 499.5 m to 500.5 m. Amplitude of power supply is 30 A with the frequency at 100 Hz. 3-D finite-difference computation will use $67 \times 67 \times 56$ grid cells, employing BICGSTAB(3) to solve the sparse system of linear equations ($m = 3$). The initial values of unknowns are all zeros . Fig. 3 shows the 3-D solution curve and 1-D solution curve of horizontal components of electric field on the survey line ($y = 100$) as well as their relative error curves. Their relative error is less than 2%. The two solutions are in very good agreement.

To further prove that the method in this paper is correct, next we will use relative residual $\varepsilon = \left\| \tilde{\mathbf{A}}\boldsymbol{x} - \tilde{\boldsymbol{b}} \right\| / \left\| \tilde{\boldsymbol{b}} \right\|$ in % to quantitatively describe the convergence of iteration, in which $\tilde{\mathbf{A}}$ and $\tilde{\boldsymbol{b}}$ represent the preconditioned coefficient matrix and the right side of Eq. (6), respectively. Fig. 4 shows the curve of iterative changes of relative residual, from

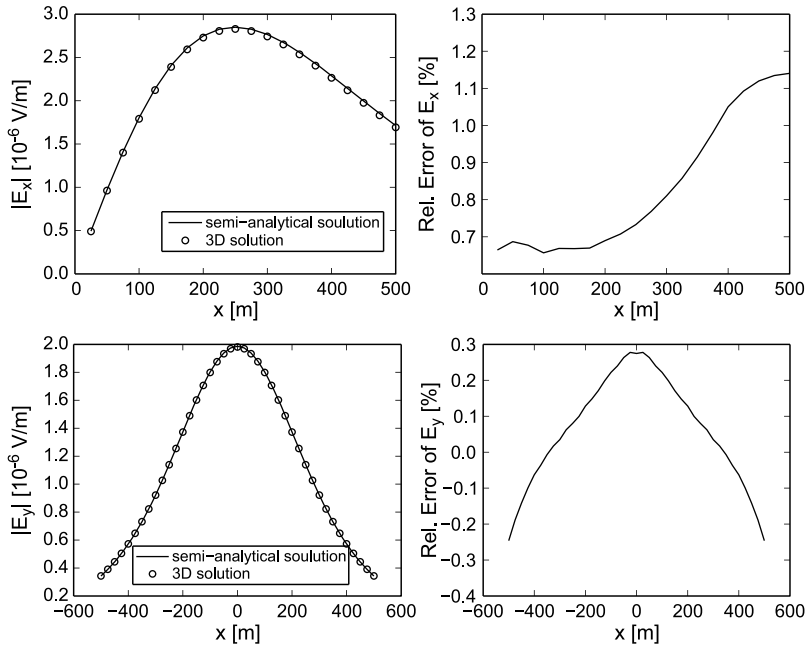

Fig. 3. Results of 3-D solution and 1-D solution of electric field's horizontal components E_x and E_y, and their relative error curves.

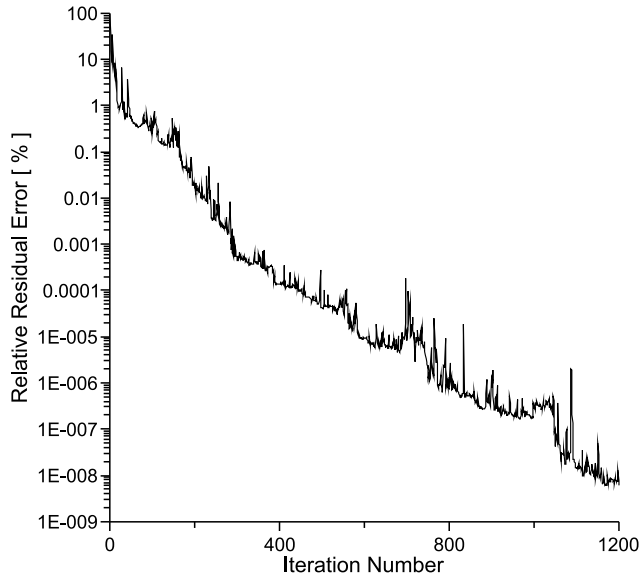

Fig. 4. Relative residual curve of iterative solution of Eq. (6).

which it can be seen that although there is local divergence, the above method displays its overall convergence, which is relatively fast.

5. PHYSICAL SIMULATIONS

For the further exploration of BSEM, in this part we will perform physical simulation, where the excitation frequency and the size of model are all designed in accordance with similarity criterion of electromagnetic simulations. Although the laboratory environment is very stable and convenient to arrange the experimental equipment and to guarantee high reproducibility of the data collection, there are limitations with regard to the simulation of the experiment sites and equipments which make collection of magnetic field signals impossible. We use medium-power electrical property magnetic transmitter, hybrid-source wide-screen electromagnetic detector, and also small-size, stable-electromotive-force calomel electrode to collect electric field signals at water surface. The set-up of this physical simulation is shown in Fig. 5.

Since oil, gas and water are to some extent non-magnetic and their magnetic permeabilities is close to vacuum permeability μ_0. BSEM field construction often uses excitation frequency in the range of 1/256 ~ 256 Hz (*Liu et al., 2006*). Then based on the size of the tank and the permeability parameters of experimental materials, we transmit the 16 × 1024 Hz periodical positive and negative pulse of square wave, and the similarity criterion (*Frischknecht, 1988*) is simplified to:

$$\sigma_m f_m L_m^2 = \sigma_f f_f L_f^2 , \tag{7}$$

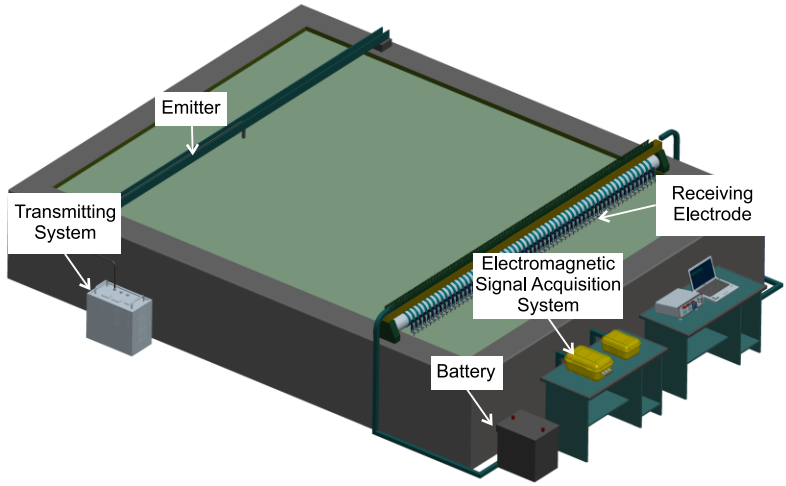

Fig. 5. Scheme of BSEM laboratory simulation set-up.

where σ is the conductivity, f is the frequency, L is the linear dimensions of modeland, subscript m represents the simulation system, while subscript f represents the corresponding on-site system of the simulation m.

In Eq. (7), set the scale to 1:400, the tank is 5.0 m long, 3.8 m wide, and 2.7 m high. We add salt water with resistivity of 2 Ωm. Taking various aspects like the particular situation of field constructions, the excitation frequency of the transmitter and the size of the tank into consideration, for the simulation of oil-and-air reservoir, we place a $0.50 \times 0.50 \times 0.15$ m cement slab mixed with a small amount of graphite 0.45 m under water, and its resistivity is 2.0×10^3 Ωm.

The upper and lower endpoints of the vertical finite line source are located at 0.36 m and 0.56 m underwater, respectively. 24 pairs of calomel electrodes, with 0.10 m interval, are placed to collect electric field signals in y direction at water surface. Here we assume the surface of water in the tank is the plane ($z = 0$) of a Cartesian coordinate system, the longer edge of the tank is in the x direction and the origin is the surface projection of vertical finite line source. Fig 6 presents two models, the first one with the vertical finite line source passing through the centre of the anomaly and the other one with the source placed outside of the anomaly. In this figure, the purple point represents the projection of vertical finite line source, and the dotted lines are the projections of 4 survey lines at water surface along x direction.

The electric field responses of y-component amplitudes of total field and primary field are measured in two different conditions - when the anomaly exists and when it does not exist. Following steps are conducted successively: trace editing, computing dominant frequency after subtracting the primary field from the total field to get the anomalous response. Two models with frequency under 16×1024 Hz are shown in Fig. 7. This figure represents the curve of anomalous field response amplitude of E_y component in y

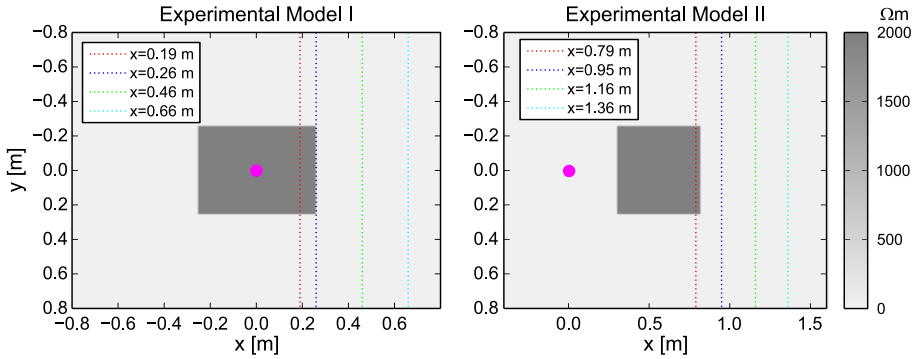

Fig. 6. Distribution of resistivity and survey lines in *x*-*y* plane of laboratory simulations ($z = 0.8$ m). The purple dot represents projection of the vertical line source on the *x*-*y* plane (surface). The grey rectangle represents surface projection of the subsurface anomaly.

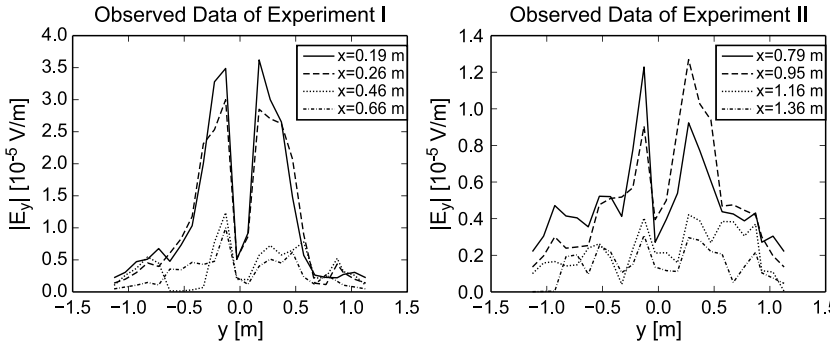

Fig. 7. Curves of anomalous field responses of E_y component of two laboratory simulations from Fig. 6.

direction of 4 survey lines. Although there are only 24 data each line, and they are also influenced by experimental errors and effects of noise, each curve is symmetrical about *y* axis. At $y = 0$ m, electric field in *y* direction is very small. But at its two sides, the anomalous response amplitude is large enough to display the existence of anomaly.

6. NUMERICAL SIMULATIONS BASED ON PHYSICAL EXPERIMENTS MODELS

Base on Eq. (7), assume the frequency of numerical simulation is 8 Hz. The dimensional ratio between physical model and numerical model is set as 1:400. Therefore the resistivity value of primary half-space model is 39.0625 Ωm; The resistivity of the anomaly is 39062.5 Ωm; The depths of two end points of the source are 144 m and 224 m, respectively. The depth of the 3-D anomaly is at 180 m. Fig. 8 shows the resistivity distribution and survey lines of horizontal profile of numerical simulation models corresponding to the two physical simulation models.

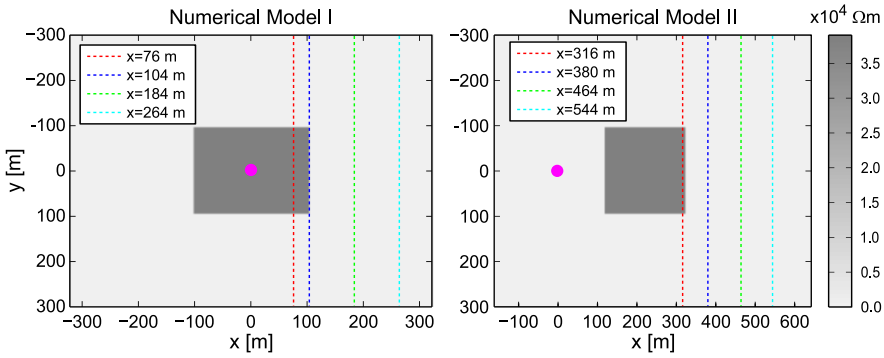

Fig. 8. The same as in Fig. 6, but for $z = 350$ m.

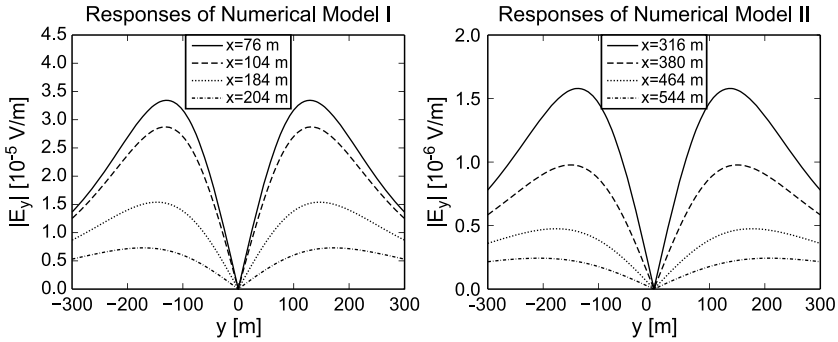

Fig. 9. Curves of anomalous field responses of E_y component of two laboratory simulations from Fig. 8.

3-D finite-difference calculation uses a 79 × 79 × 78 grid. Fig. 9 is the anomalous field response amplitude curve of E_y component in y direction, which is symmetric about the origin. And the anomalous response curve of near-field survey line has a very clear peak while the curve of far-field is more smooth, yet covering a larger anomalous area. Comparing with Fig. 7, it can be seen that these response curves under 4 conditions are consistent with each other; anomalous electric field is symmetrical about the vertical finite line source, displaying dipole structure. All of these similarities validate each other, proving that the numerical simulations and the physical simulations are correct, and that BSEM is a strong weapon to prospect high-resistivity oil and gas reservoirs.

To research on response characters of anomalies of different resistivity, Model II will be used to calculate the numerical responses of three anomalous fields with different resistivity. In Fig. 10, curves in three conditions share similar shape. And the amplitude curve of anomalous field of component E_x displays unimodal structure while on the part of E_y component, it keeps a bimodal structure, both of which demonstrate the existence of anomalies. The higher the resistivity of anomaly increases, the more obvious the anomaly of near-source area becomes, which proves that BSEM is suitable for prospecting high-resistivity oil-and-gas reservoir.

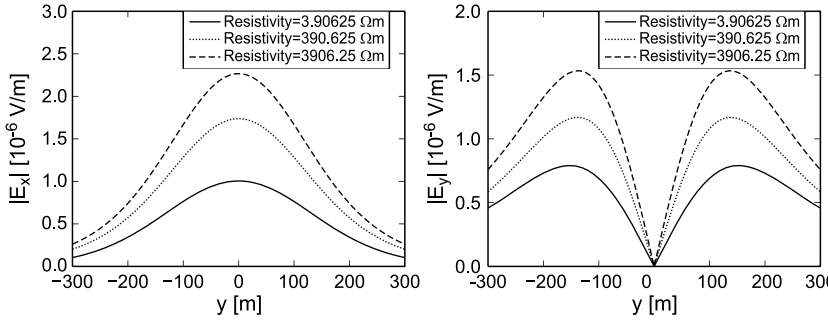

Fig. 10. Response curves of anomalous field of components E_x and E_y on survey line (x = 316 m) with varying resistivity.

7. 3-D TARGET NUMERICAL SIMULATION EXAMPLE

In a homogeneous half-space, a cube with side length of 1000 m and resistivity of 20 Ωm is placed at the location defined by [1000, 2000] × [−500, 500] × [1000, 2000] m. The length of vertical finite line source is 1000 m (i.e. $h_2 - h_1 = 1000$ m) with the coordinates of upper and lower end points being $(0, 0, h_1)$ and $(0, 0, h_2)$. Intensity of electric current is 10 A, and the frequency is 100 Hz. Fig. 11 displays the response distribution of total field $|E_x|$ at the surface generated by vertical finite line source at different depths. The purple circle is the projection of the source while the square frame is the projection of the anomaly at the surface. From the figure, it can be learnt that the impact of the anomaly on currents is relatively small when the source is shallower than the anomaly, and the field that can be observed at the surface is mainly the primary field (Fig. 11a); the impact of source on total field observed at the surface becomes smaller as the depth of the source increases, at the same time, the anomalous field is easier to be observed, showing the anomaly and its distribution (Fig. 11b,c).

Under the three conditions above, the distribution of component $|E_x|$ total field responses of the profile (y = 500) is given in Fig. 12. The black vertical line on the left is the vertical finite line source, while the black square frame is the projection of anomaly. To display the distribution of field more straightforward, here we will take the log of field value. It is clear that when the depth of source is relatively shallower than that of anomaly, the responses on the surface is mainly from the primary field, and the amplitude of the near-source field on the upper left corner of anomaly grows relatively bigger (Fig. 12a); when the depth of source is the same as the depth of anomaly, the field amplitude on the upper- and lower-left corner of anomaly is almost the same too, but the response of anomaly field measured at the surface gets stronger (Fig. 12b); when the source goes more deeper than the anomaly does, the amplitude of the near-source field on the lower left corner of anomaly becomes bigger, and the response of anomaly field can to some extent be clearly measured on the surface (Fig. 12c), too. So it is safe to tell that BSEM not only can gain subsurface anomalous information by varying transmitting frequency, but also can gain information about subsurface medium from different angles by changing the

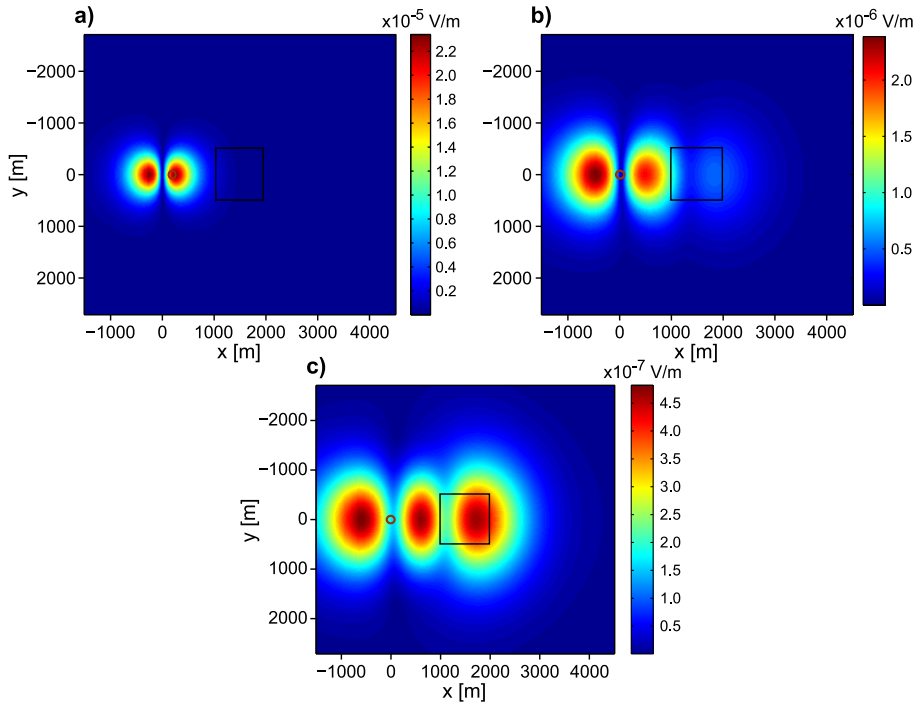

Fig. 11. Response distribution of surface total field $|E_x|$ generated by vertical finite line source between depths: **a)** $h_1 = 500$ m, $h_2 = 1500$ m, **b)** $h_1 = 1000$ m, $h_2 = 2000$ m, **c)** $h_1 = 1500$ m, $h_2 = 2500$ m. The red circle and black rectangle represent the projection of the vertical line source and underground abnormal structure on the surface, respectively.

position of transmission source in the borehole, which will facilitate the interpretation of inversion.

8. CONCLUSIONS

This paper uses frequency-domain staggered-grid finite differential method to perform 3-D BSEM forward simulation. The method is proved to converge in the iterative process and is fast and reliable. Additionally, we also perform a physical laboratory simulation and compare its results with those of a numerical model designed according to similarity criterions. The models make it possible to assess the impact area of the anomaly. The result demonstrates that, in addition to the information obtained from responses at different frequencies, BSEM can also make use of various locations of the excitation source and measure response data of surface electromagnetic field components to produce high-accuracy results about subsurface anomaly, which justifies the method as an efficient tool to detect high-resistivity oil and gas reservoir. The numerical and physical simulation in this paper will enrich studies on BSEM, and further support studies on electromagnetic response of oil and gas reservoir in complex geological conditions.

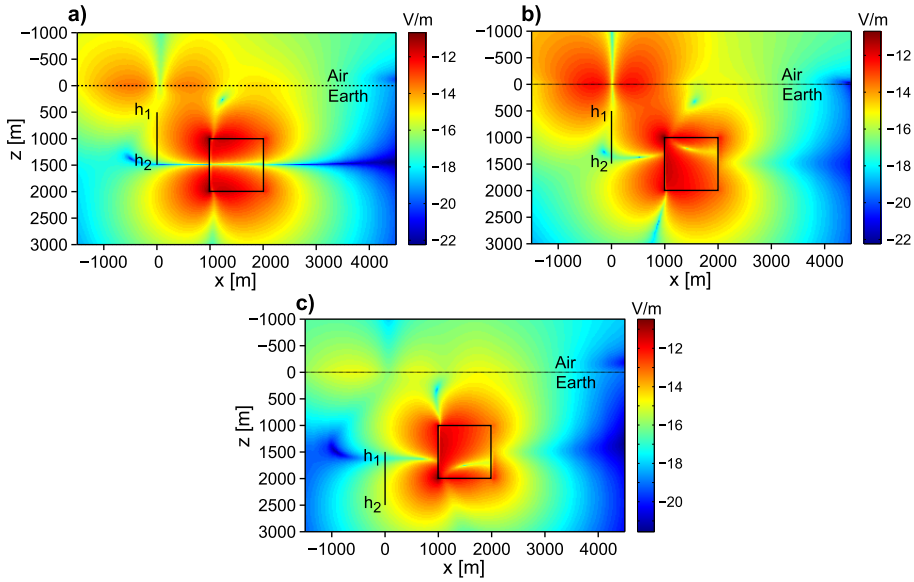

Fig. 12. Distribution of logarithm of $|E_x|$ component of total field responses along the profile at $y = 500$ m, when vertical finite line source is between different depths: **a)** $h_1 = 500$ m, $h_2 = 1500$ m, **b)** $h_1 = 1000$ m, $h_2 = 2000$ m, **c)** $h_1 = 1500$ m, $h_2 = 2500$ m. The red circle and black rectangle represent the projection of the vertical line source and underground abnormal structure on the surface, respectively.

Acknowledgements: This study was supported by the NSFC projects No. u1262206 and 41174092. The author wishes to thank the Key Laboratory of Earth Exploration and Information Techniques of Ministry of Education in CDUT, the Geophysical and Geochemical Exploration Department of BGP INC., China National Petroleum Corporation, and its work group as well. At the same time, the author also thanks the associate editor Dr. Josef Pek, Dr. Jakub Velimský, and another anonymous reviewer for their valuable suggestions on this paper.

References

An R., Li T. and Xu K., 2007. Well-surface 3-D resistivity inversion. Progr. Geophys., **22** 247–249.

Badea E.A., Everett M.E., Newman G.A. and Biro O., 2001. Finite-element analysis of controlled-source electromagnetic induction using Coulomb-gauged potentials. *Geophysics*, **66**, 786–799.

Cao H., Wang X. and He Z., 2012. Borehole-to-surface electromagnetic responses of the horizontally stratified medium. *Oil Geophys. Prospect.*, **47**, 338–343.

Champagne N.J., Berryman J.G. and Buettner H.M., 2001. FDFD: A 3D finite-difference frequency-domain code for electromagnetic induction tomography. *J. Comput. Phys*., **170**, 830–848.

Freund R., 1993. A transpose-free quasi-minimal residual algorithm for non-Hermitian linear systems. *SIAM J. Sci. Comput*, **14**, 470–482.

Frischknecht F.C., 1988. Electromagnetic physical scale modeling. In: Nabighian M.S. (Ed.), *Electromagnetic Methods in Applied Geophysics, Volume I, Theory*. Society of Exploration Geophysicists, Tulsa, OK, 365–441.

Guptasarma D. and Singh B., 1997. New digital linear filters for Hankel J0 and J1 transforms. *Geophys. Prospect.*, **45**, 745–762.

Hohmann G.W., 1975. Three-dimensional induced polarization and EM modeling. *Geophysics*, **40**, 309–324.

Ke G. and Huang Q., 2009. 3D forward and inversion problems of borehole-to-surface electrical method. *Acta Scientiarum Naturalium Universitatis Pekinensis*, **45**, 264–272.

Key K., 2009. 1D Inversion of multi-component, multi-frequency marine CSEM data, methodology and synthetic studies for resolving thin resistive layers. *Geophysics*, **74**, F9–F20.

Liu C., Ren Z., Tang J. and Yan L., 2008.Three-dimensional magnetotellurics modeling using edge-based finite-element unstructured meshes. *Appl. Geophys*., **5**, 170–180.

Liu X., Wang J., He Z. and Wang Z., 2006. Study of hydrocarbon accumulation by borehole-ground EM method. *Progr. Explor. Geophys*., **29**, 98–101.

Mitsuhata Y. and Uchida T., 2004. 3D magnetotelluric modeling using the T-Ω finite-element method. *Geophysics*, **69**, 108–119.

Newman G.A. and Alumbaugh D.L., 1995. Frequency-domain modeling of airborne electromagnetic responses using staggered finite differences. Geophys. Prospect., **43**, 1021–1041.

Newman G.A., Hohmann G.W. and Anderson W.L., 1986. Transient electromagnetic response of the three-dimensional body in a layered Earth. *Geophysics*, **51**, 1608–1627.

Sleijpen G.L.G. and Fokkema D.R., 1993. BICGSTAB(L) for linear equations involving unsymmetric matrices with complex spectrum. *Electron. Trans. Numer. Anal.*, **1**, 11–32.

Streich R., 2009. 3D Finite-difference frequency-domain modeling of controlled-source electromagnetic data. Direct solution and optimization for high accuracy. *Geophysics*, **74**, 95–105.

Tripp A.C. and Hohmann G.W., 1984. Block diagonalization of the electromagnetic impedance matrix of a symmetric buried body using group theory. *IEEE Trans. Geosci. Remote Sens.*, **22**, 62–69.

Wang Z., He Z. and Liu Y., 2006. Research of 3D modeling and anomalous rule on borehole-ground DC method. *Chinese J. Eng. Geophys.*, **3**, 87–92.

Wang Z., He Z. and Wei W., 2007a. 3D modeling and Born approximation inversion for the borehole surface electromagnetic method. *Appl. Geophys.*, **4**, 84–88.

Wang Z., He Z. and Wei W., 2007b. Parallel algorithm research of integral equation method to 3D borehole-surface electromagnetic modeling. *Comput. Techn. Geophys. Geochem. Explor.*, **29**, 425–430.

Wang Z., He Z., Wei W. and Deng M., 2005. 3D physical model experiments of well-to-ground electrical survey. *Oil Geophys. Prospect.*, **40**, 594–597.

Xiong Z., 1992. Electromagnetic modeling of 3D structures by the method of system iteration using integral equations. *Geophysics*, **57**, 1556–1561.

Xu K. and Li T., 2006. The forward modeling of three-dimensional geoelectric field of vertical finite line source by finite-difference method. *J. Jilin Univ. (Earth Sci.)*, **36**, 137–141.

Zhdanov M.S. and Fang S., 1997. Quasi-linear series in three-dimensional electromagnetic modeling. *Radio Sci.*, **31**, 741–754.

Zhang T. and Zhang B., 1995. Research on removing noises in DC resitivity trielectrode gradient measurement. *Oil Geophys. Prospect.*, **30**, 100–110.

Yee K., 1966. Numerical solution of initial boundary value problems involving Maxwell's equations in isotropic media. *IEEE Trans. Antennas Propag.*, **16**, 302–307.